Inorganic Chemistry

pubs.acs.org/IC

Article

Characterization of and Structural Insight into Struvite-K, $MgKPO_4{\cdot}6H_2O$, an Analogue of Struvite

Laura J. Gardner, Samuel A. Walling, Sebastian M. Lawson, Shikuan Sun, Susan A. Bernal, Claire L. Corkhill, John L. Provis, David C. Apperley, Dinu Iuga, John V. Hanna, and Neil C. Hyatt*

Cite This: *Inorg. Chem.* 2021, 60, 195−205

Read Online

ACCESS | Metrics & More | Article Recommendations | Supporting Information

ABSTRACT: Struvite-K ($MgKPO_4{\cdot}6H_2O$) is a magnesium potassium phosphate mineral with naturally cementitious properties, which is finding increasing usage as an inorganic cement for niche applications including nuclear waste management and rapid road repair. Struvite-K is also of interest in sustainable phosphate recovery from wastewater and, as such, a detailed knowledge of the crystal chemistry and high-temperature behavior is required to support further laboratory investigations and industrial applications. In this study, the local chemical environments of synthetic struvite-K were investigated using high-field solid-state ^{25}Mg and ^{39}K MAS NMR techniques, alongside ^{31}P MAS NMR and thermal analysis. A single resonance was present in each of the ^{25}Mg and ^{39}K MAS NMR spectra, reported here for the first time alongside the experimental and calculated isotropic chemical shifts, which were comparable to the available data for isostructural struvite ($MgNH_4PO_4{\cdot}6H_2O$). An *in situ* high-temperature XRD analysis of struvite-K revealed the presence of a crystalline−amorphous−crystalline transition that occurred between 30 and 350 °C, following the single dehydration step of struvite-K. Between 50 and 300 °C, struvite-K dehydration yielded a transient disordered (amorphous) phase identified here for the first time, denoted δ-$MgKPO_4$. At 350 °C, recrystallization was observed, yielding β-$MgKPO_4$, commensurate with an endothermic DTA event. A subsequent phase transition to γ-$MgKPO_4$ was observed on further heating, which reversed on cooling, resulting in the α-$MgKPO_4$ structure stabilized at room temperature. This behavior was dissimilar from that of struvite exposed to high temperature, where NH_4 liberation occurs at temperatures >50 °C, indicating that struvite-K could potentially withstand high temperatures via a transition to $MgKPO_4$.

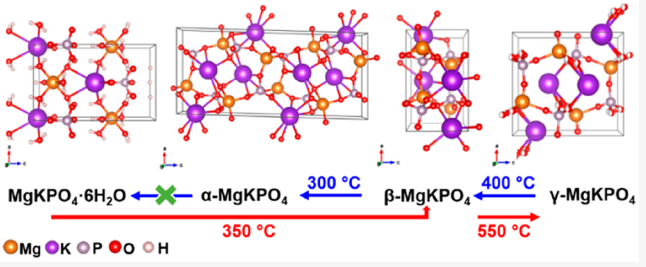

1. INTRODUCTION

The mineral struvite ($MgNH_4PO_4{\cdot}6H_2O$) was first identified in 1845 within the grounds of St. Nicholas Church, Hamburg, Germany,[1] and has since been identified in kidney stones, bat guano, and wastewater systems. Several studies have detailed the structure of struvite (orthorhombic, space group $Pmn2_1$) and its common analogues, $MgMPO_4{\cdot}6H_2O$, where M^+ is Rb^+, Cs^+, Tl^+, or K^+.[2−4] The substitution of these cations for ammonium within the struvite structure did not change the orthorhombic symmetry with the exception of Cs^+, which formed a hexagonal structure (space group $P6_3mc$) due to its larger ionic radius.[2−4] In Figure 1, the crystal structure of struvite-K ($MgKPO_4{\cdot}6H_2O$, *b* axis view) was produced using crystallographic data published by Mathew and Schroeder[3] with a reported unit cell with parameters $a = 6.873$ Å, $b = 6.160$ Å, and $c = 11.087$ Å,[3,5] which is comparable to those of struvite at $a = 6.941$ Å, $b = 6.137$ Å, and $c = 11.199$ Å.[2] Mathew and Schroeder[3] ascribed the minor structural differences between struvite and struvite-K as being due to the weak interactions between NH_4 or K and the oxygen atoms in the water molecules within the crystal structure. Since 2003, struvite-K has been classified as a natural mineral in its own right after it was discovered in two locations: Binntal, Switzerland, and the Styria region of Austria.[5]

Struvite and struvite-K form the key strength-giving constituent of magnesium phosphate cements (MPCs). These acid−base cements are formed by the reaction between dead-burnt magnesium oxide (MgO), ammonium (or potassium) dihydrogen phosphate ($NH_4H_2PO_4$, KH_2PO_4), and water, as represented in eqs 1 and 2, respectively. The use of dead-burnt MgO in MPCs results in a slower reaction in comparison to more soluble sources of magnesium, resulting in a workable cement paste (over several hours) rather than instantaneous setting.[7]

$$MgO(s) + NH_4H_2PO_4(s) + 5H_2O(l) \rightarrow MgNH_4PO_4{\cdot}6H_2O(s) \quad (1)$$

Received: September 20, 2020
Published: December 14, 2020

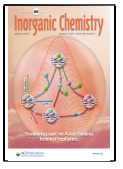

https://dx.doi.org/10.1021/acs.inorgchem.0c02802
Inorg. Chem. 2021, 60, 195−205

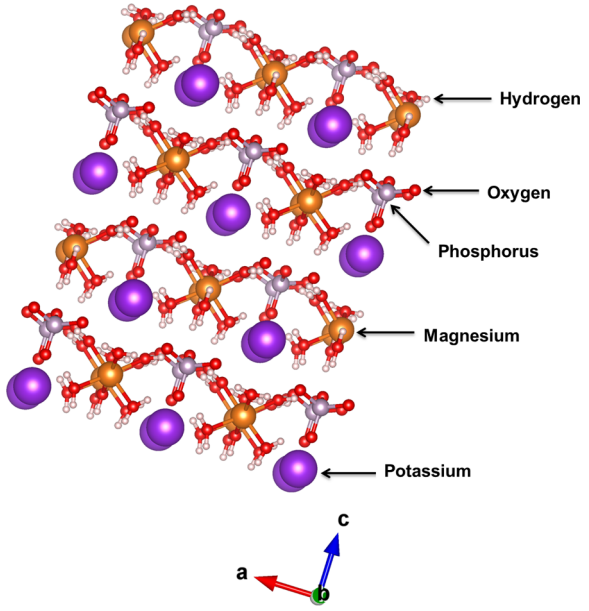

Figure 1. Crystal structure of struvite-K ($Pmn2_1$) visualized using VESTA.[6]

$$MgO(s) + KH_2PO_4(s) + 5H_2O(l) \rightarrow MgKPO_4{\cdot}6H_2O(s) \quad (2)$$

While initially finding use as a rapid patch repair material (roads, bridges, runways, etc.), struvite cement has become less popular in favor of the struvite-K system, which does not release ammonia during setting and has slower (although still relatively fast) setting characteristics. These advantages have opened new applications on the basis of the near-neutral pH property of struvite-K cements, including the immobilization of certain radioactive wastes,[7−14] particularly reactive metals and other problematic waste streams that are not compatible with conventional Portland cement encapsulation. Other applications include fiber−cement composites[15−18] (e.g., glass fiber and mineral wools, which may react in conventional cements), internal concrete repair/bonding,[19−21] and the stabilization of contaminated soils.[22,23] Aside from the cementitious properties, there is also interest in the chemistry of struvite-K (alongside struvite and Na-struvite) to facilitate phosphate removal from wastewaters,[24−26] as part of global efforts toward sustainable stewardship of phosphate resources.

Due to the increased interest in struvite-K-based cements, it is important to understand the local chemical environments and high-temperature stability of this mineral to underpin any applications of this material. This detailed structural insight could contribute toward the continued development of magnesium potassium phosphate cements (MKPCs) for radioactive waste immobilization and struvite-K formation in phosphate recovery applications. As such, high-field (19.96 T) ^{25}Mg and ^{39}K magic angle spinning (MAS) nuclear magnetic resonance (NMR) data are presented herein, in addition to ^{31}P MAS NMR spectra, X-ray diffraction (XRD), thermal analysis, and *in situ* high-temperature XRD data (HTXRD), to enable more precise characterization of the structure and behavior of struvite-K.

2. EXPERIMENTAL SECTION

2.1. Materials and Methods. The struvite-K precursors were as follows: KH_2PO_4 (>99% purity, Prayon), available as Food grade E340 MKP; $MgCl_2$ (anhydrous, ≥98% purity, Sigma-Aldrich); KOH solution (45 wt % in H_2O, Sigma-Aldrich); deionized H_2O. Struvite-K synthesis (eq 3) was undertaken directly as described by Mathew and Schroeder.[3] A solution was prepared in a conical flask with 25 g of KH_2PO_4 (0.1837 mol), 5 g of $MgCl_2$ (0.0525 mol), and 100 mL of deionized H_2O. The stoichiometric reaction is based on a 1:1 magnesium to phosphate (Mg:P) molar ratio (eq 3); however, excess KH_2PO_4 was utilized, equivalent to a 1:3.5 Mg:P molar ratio. No explanation was provided by Mathew and Schroeder;[3] however, we postulate that excess KH_2PO_4 was included to ensure the maximum uptake of Mg within struvite-K ($MgKPO_4{\cdot}6H_2O$) was achieved. Once the solution was prepared, it was stirred for 10 min before the conical flask was transferred to a clamp stand and positioned in an angled position (~45°). The initial solution was recorded to be pH 4.4, which was adjusted by the addition of KOH (45 wt % in H_2O, 11.7 M) in 1−2 mL increments until pH 7.5 was achieved. In total ~20 mL was required, with the pH measured using a three-point calibrated pH probe subsequent to each 1−2 mL KOH addition. Immediately upon the addition of KOH, a white precipitate began to appear. The solution was held static for 7 days at room temperature, allowing for the reaction to complete. The white precipitate was vacuum-filtered and washed multiple times with deionized H_2O followed by a final acetone wash. The struvite-K powder was transferred to a vacuum desiccator to dry for 2 days prior to characterization. The struvite-K synthesis produced 13.61 g (0.0511 mol), which was equivalent to a yield of 97.26%, on the basis of the limited availability of Mg ($MgCl_2$; 0.0525 mol).

$$MgCl_2(s) + KH_2PO_4(s) + 6H_2O(l) + 2KOH(aq) \rightarrow MgKPO_4{\cdot}6H_2O(s) + 2KCl(aq) + 2H_2O(l) \quad (3)$$

2.2. Analytical Methods. The struvite-K powder was ground using an agate mortar and sieved through a 63 μm brass sieve prior to analysis. SEM analysis was performed using a Hitachi TM3030 analytical benchtop SEM apparatus with an integrated Bruker EDX system (Quantax 70) at 15 kV and a 7.0 mm working distance. The SEM sample was prepared by lightly dusting the sieved powder onto an adhesive carbon tab and aluminum pin stud; no additional sample preparation techniques (i.e. polishing and carbon coating) were used. Thermal analysis data were collected using Pyris 1 TGA and PerkinElmer DTA 7 instruments, in alumina crucibles under a N_2 atmosphere at 10 °C/min, up to 1000 °C.

Solid-state ^{31}P MAS NMR data were acquired at 9.4 T (Larmor frequency ν_0 = 161.87 MHz) using a Varian VNMRS-400 spectrometer and a 4 mm Varian MAS NMR probe, which enabled rotational frequencies of 10 kHz for all measurements. The ^{31}P MAS NMR single-pulse excitation data were measured using a $\pi/2$ pulse duration of 4.4 μs with a ^{31}P acquisition time of 30 ms and a relaxation time of 300 s (eight scans per spectrum), while the $^{1}H-^{31}P$ cross-polarization (CPMAS) NMR data were acquired using an initial ^{1}H $\pi/2$ pulse duration of 4.4 μs, a Hartmann−Hahn contact period of 1 ms, an acquisition time of 30 ms, and a recycle delay of 300 s. All ^{31}P chemical shifts were referenced externally to the IUPAC primary reference of 85% H_3PO_4 (δ 0.0 ppm) via a secondary solid reference of ammonium dihydrate phosphate ($NH_4H_2PO_4$, δ 0.99 ppm). The MAS NMR measurement of low-γ quadrupolar nuclei, ^{25}Mg and ^{39}K, were undertaken at high field (20.0 T) using a Bruker Avance III-850 spectrometer operating at Larmor frequencies (ν_0) of 52.02 and 39.68 MHz, respectively. The low natural abundance and moderate quadrupole moment (Q) of the ^{25}Mg nucleus and the very low sensitivity (and often long T_1s) of the ^{39}K nucleus necessitate the study of these nuclei at the highest available field strengths. Both nuclei were studied using a Bruker low-γ 4 mm HX probe using MAS frequencies of 10 kHz for the ^{25}Mg MAS NMR and 15 kHz for ^{39}K MAS NMR.

The ^{25}Mg MAS NMR study of struvite-K was undertaken using double frequency sweep (DFS) detection using a 2 ms DFS enhancement of the central transition[27] followed by a 5.0 μs (90°) excitation pulse. A total of 8192 transients were acquired using a recycle time of 2.0 s. The reported ^{25}Mg isotropic chemical shifts (δ_{iso}) were externally referenced to the IUPAC reference of 3 M $MgSO_4$(aq) (δ_{iso} 0.0 ppm) via a secondary solid MgO reference (δ_{iso} 26.0 ppm).[28] The

https://dx.doi.org/10.1021/acs.inorgchem.0c02802
Inorg. Chem. 2021, 60, 195−205

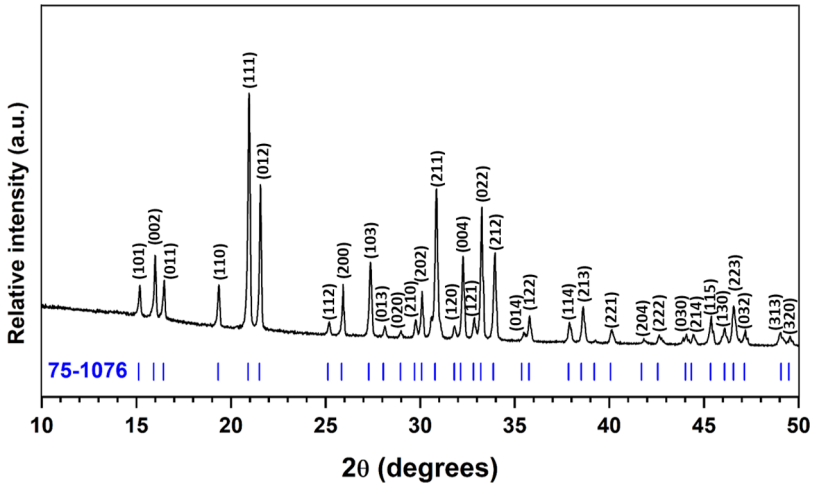

Figure 2. X-ray diffraction pattern collected for struvite-K in the range $10° \leq 2\theta \leq 50°$ at 30 °C. The reflections (blue tick marks) and Miller indices are indexed to those reported by Mathew and Schroeder (PDF #75-1076).[3]

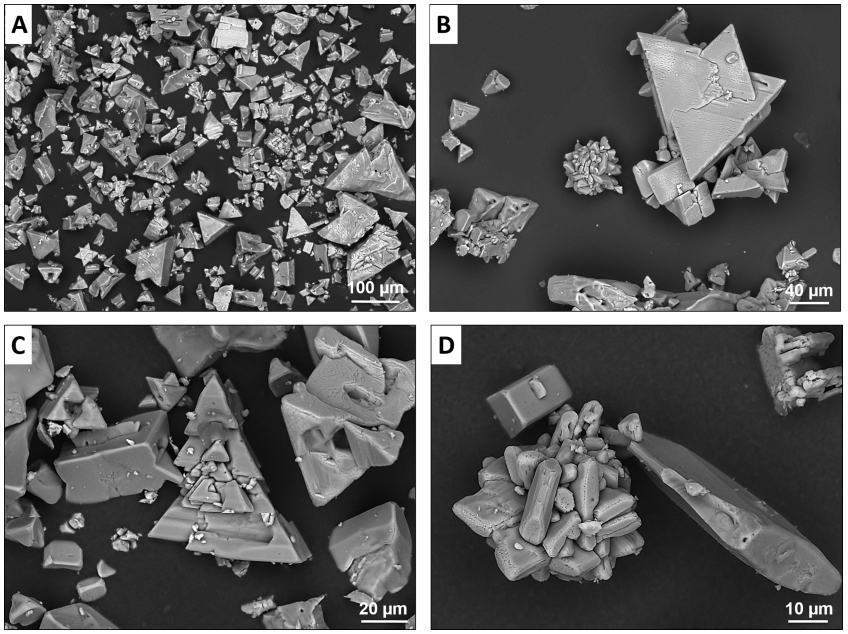

Figure 3. BSE micrographs of struvite-K at different magnifications.

corresponding ^{39}K MAS NMR study was undertaken using a Hahn echo[29] pulse sequence using 15.0 μs (90°) and 30 μs (180 °) pulses preceded by 2 ms DFS enhancement of the central transition. A total of 46080 scans were acquired using an echo time of 1 rotor period and a recycle time of 2.0 s. The reported ^{39}K isotropic chemical shifts (δ_{iso}) were externally referenced to the IUPAC reference of 1 M KCl(aq) (δ_{iso} 0.0 ppm) via a secondary solid KCl reference (δ_{iso} 42.0 ppm).[30] The acquired ^{25}Mg and ^{39}K MAS NMR spectra were simulated using Bruker TopSpin 3.2 software,[31] where only the second-order broadened central transition line shapes were considered.

In situ high-temperature XRD (HTXRD) data were acquired using a PANalytical X'Pert3 powder diffractometer, in reflection mode, with an Anton Parr HTK 1200N furnace. HTXRD data were acquired in the range 30−1000 °C, in the range $10° \leq 2\theta \leq 50°$, with Cu K$\alpha$ radiation (1.5418 Å), step size 0.02°, time per step 3 s, and a ramp rate of 10 °C/min (controlled for both the heating and cooling stages using a PID controller) in an alumina crucible. The temperature was held for 5 min prior to data collection in order to ensure that a stabilized temperature was achieved. Le Bail profile fitting was used to calculate sample unit cell volumes and was performed using the Bruker TOPAS software package. Rietveld refinements were performed at key *in situ* heating and cooling temperatures using GSAS software to determine the correct structural assignments for *in situ* HTXRD patterns (β-$MgKPO_4$ or γ-$MgKPO_4$). To assist refinement, isostructural compounds with the structures $Pna2_1$[32] and *Pnma*[33] were used to generate diffraction patterns for a comparison to experimental data.

3. RESULTS AND DISCUSSION

3.1. Struvite-K. The diffraction pattern for struvite-K (Figure 2) was in agreement with the diffraction patterns reported by Mathew and Schroeder[3] and Graeser et al.,[5] the latter being a natural struvite-K source. No evidence of any unreacted reacted precursors ($MgCl_2$, KH_2PO_4) was observed in the XRD data, suggesting a complete reaction. In SEM micrographs (Figure 3), struvite-K was found to have a prismatic crystal habit with a mixture of triangular prisms, cuboids, and aggregated closely spaced tabular crystals, with a broad size variation between 10 and 180 μm (Figure 3A). The crystal habit of natural struvite-K mineral sources was described as being flat tabular crystals with wedge-shaped edges elongated along the

https://dx.doi.org/10.1021/acs.inorgchem.0c02802
Inorg. Chem. 2021, 60, 195−205

crystallographic *a* axis.[5] These descriptions could be ascribed to the morphologies observed in Figure 3B,D. It is postulated that the combination of uniform and isosceles triangular prisms found in Figure 3A−C is akin to the tetrahedral disphenoid typically reported for synthetic struvite-K.[3] The EDX spectrum presented in Figure S1 is representative of the bulk struvite-K crystals (measured across a range of micrographs; only one shown) with emission energies only being observed for the expected elements: Mg, K, P, and O. Semiquantitative phase analysis determined the average struvite-K composition to be $Mg_{0.98(3)}K_{1.06(7)}P_{(0.96(6)}O_4{\cdot}6H_2O$, which was in close agreement with the targeted stoichiometry, $MgKPO_4{\cdot}6H_2O$. The calculated composition was determined on the basis of the Mg:K:P cation ratio (derived from the normalized atomic percentages) across 10 spot analyses ±1 standard deviation.

3.2. Solid-State Nuclear Magnetic Spectroscopy. The local chemical environments present within struvite-K were determined using ^{31}P, ^{25}Mg, and ^{39}K MAS NMR spectroscopy (Figure 4). The ^{31}P MAS NMR spectrum (Figure 4A) exhibited a single sharp resonance centered at 6.2 ppm in the orthophosphate region, which was associated with crystalline struvite-K and was similar to isostructural struvite at 6.1 ppm,[34−36] confirming that both minerals have only one P site. Alongside the ^{31}P MAS NMR data, cross-polarization with ^{1}H CP/MAS NMR was performed to observe hydrated phosphate phases within the struvite-K. In Figure 4A, the CP/MAS NMR spectrum clearly shows a single sharp resonance (at 6.2 ppm), which indicates that all of the P−H interactions within this specimen were associated with the hexahydrate struvite-K phase. There is a very low intensity resonance around ∼3.8 ppm present in both the MAS and $^{1}H-^{31}P$ CP spectra that could be associated with the phosphate precursor (KH_2PO_4, δ 3.6 ppm, collected during this study). However, there was no evidence of KH_2PO_4 in the diffraction pattern (Figure 2), consistent with the presence of a trace quantity below the detection limit.

The ^{25}Mg and ^{39}K MAS NMR nuclei both have quadrupole moments (spins 5/2 and 3/2, respectively) interacting with the electric field gradient,[37] which can be mitigated by high-field MAS NMR. The characteristic resonance shapes observed in Figure 4B,C clearly indicated that the ^{25}Mg and ^{39}K environments in struvite-K still experienced broadening due to second-order quadrupolar interactions.[28] The ^{25}Mg MAS NMR spectrum of synthetic struvite-K (Figure 4B) identified a single resonance (second-order line shape) centered at δ_{iso} −1.0 ppm, which was associated with octahedrally coordinated Mg observed as $Mg(H_2O)_6$ species in the crystal structure (Figure 1). The simulated spectrum (blue line) was in agreement with the presence of a single Mg site in struvite-K. An empirical fitting method was used in Topspin 3.2[31] to simulate the experimental spectrum for the observed nuclei and to determine the quadrupolar parameters (Table 1): isotropic chemical shift (δ_{iso}), quadrupolar coupling constant (C_Q), and asymmetry (η_Q). The calculated ^{25}Mg quadrupolar parameters of struvite-K were found to be comparable to those for struvite, which are reported as 1.0 ppm (δ_{iso}), 3.56 MHz (C_Q), and 0.34 (η_Q).[28] These data concur with the interpretation of Mathew and Schroeder,[3] that the replacement of NH_4^+ with K^+ (from struvite to struvite-K) only results in minor structural changes due to the differences in ionic radii, from 1.61 Å[38] to 1.38 Å,[39] respectively. These changes do not appear to affect the Mg−O bond lengths, which have interatomic distances (mean values) of 2.071 Å for struvite-K[3] and 2.072 Å for struvite.[2]

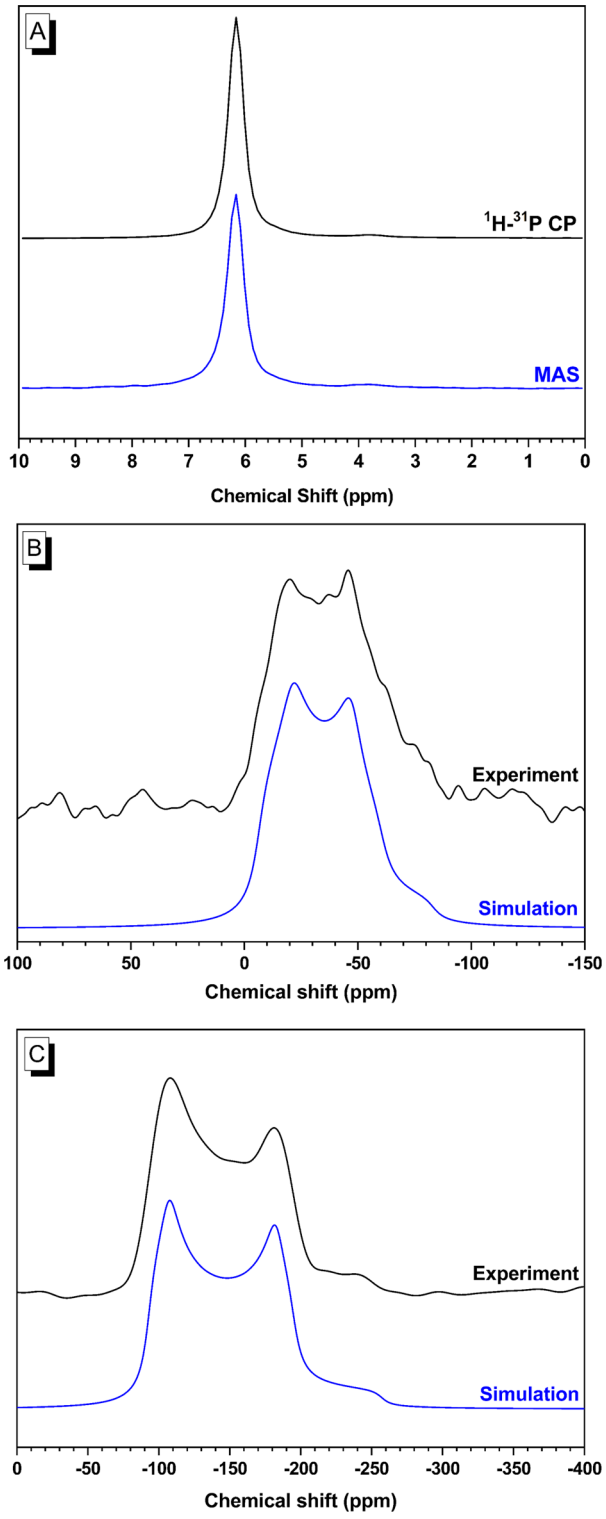

Figure 4. NMR spectra of Struvite-K local environments for (A) ^{31}P MAS and $^{1}H-^{31}P$ CP/MAS, (B) ^{25}Mg MAS, and (C) ^{39}K MAS. Simulations were performed considering the second-order quadrupolar interaction for the central transition only.

The ^{39}K MAS NMR spectrum (Figure 4C) exhibited only a single resonance (with a second-order line shape representative of an ordered compound) centered at δ_{iso} −73.1 ppm that was solely assigned to struvite-K, where the K^+ ion was bonded to five O atoms: one from a PO_4^{3-} unit and the remaining from

https://dx.doi.org/10.1021/acs.inorgchem.0c02802
Inorg. Chem. 2021, 60, 195−205

Table 1. NMR Quadrupolar Parameters for Sites in Synthetic Struvite-K, Determined by Fitting to High-Field ^{25}Mg and ^{39}K MAS NMR Data

	experimental NMR		
site	δ_{iso} (ppm) (±0.1)	C_Q (MHz) (±0.1)	η_Q (±0.02)
Mg	−1.0	3.8	0.33
K	−73.1	2.2	0.14

H_2O molecules.[3] The quadrupolar parameters from ^{39}K MAS NMR that represent pure struvite-K are shown in Table 1.

3.3. Thermal Analysis. Thermogravimetric analysis (TGA/DTG) of struvite-K (Figure 5A) revealed the occurrence of a

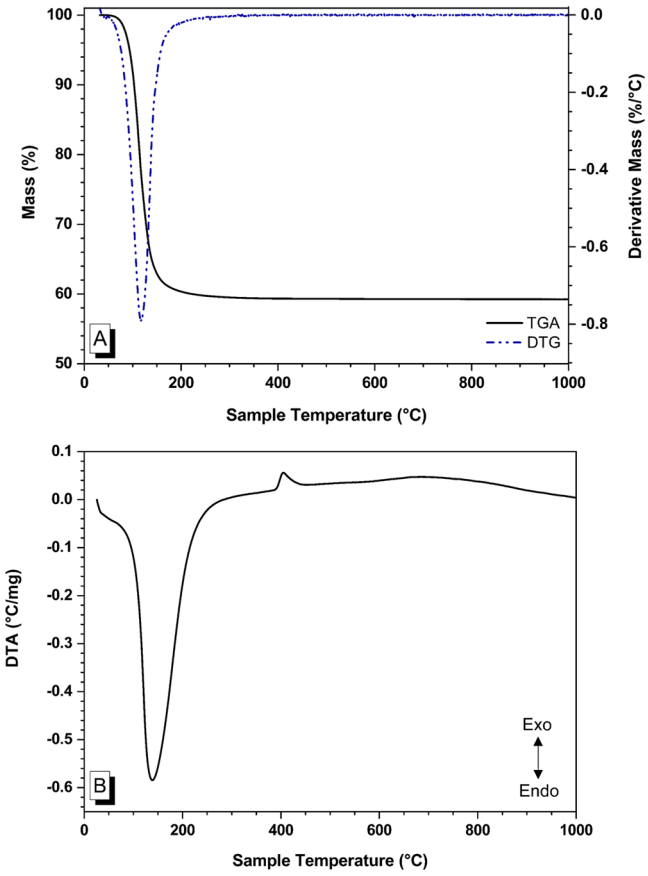

Figure 5. (A) Thermogravimetric analysis of struvite-K (black solid line), where the blue dotted line represents the first derivative thermogravimetic analysis (DTG) trace. (B) Differential thermal analysis trace of struvite-K.

single, significant mass loss (39.73%) between 40 and 200 °C. This event corresponds to the one-step dehydration of struvite-K (eq 4) reported in the literature for both struvite-K[40,41] and magnesium potassium phosphate cements.[42−45] Differential thermal analysis (DTA) revealed that an endothermic event linked to the dehydration of struvite-K occurred between 150 and 200 °C (Figure 5B), confirming the one-step dehydration process. Beyond 200 °C, however, an exothermic event (with no mass loss; Figure 5B) was observed between 380 and 445 °C and centered at 405 °C in the DTA thermogram. Similar events have been recognized in other MKPC systems (albeit with differing molar ratios, water contents, and fillers), where the DSC/DTA temperature range reported exceeds >400 °C.[41,46−50] Little explanation was provided to account for this observation: the exotherm was proposed to be associated with a possible phase transition,[41] but no evidence was provided to support this statement. To elucidate the origin of this distinct DTA feature, *in situ* high-temperature XRD data will be presented in the following section.

$$MgKPO_4{\cdot}6H_2O(s) \rightarrow MgKPO_4(s) + 6H_2O(g) \quad (4)$$

3.4. *In Situ* High-Temperature Behavior of Struvite-K. *In situ* high-temperature XRD (HTXRD) was used to determine the temperature behavior of struvite-K and to establish the origin of the DTA exothermic event observed in Figure 5B. In the diffraction pattern of struvite-K at 50 °C (Figure 6), only reflections corresponding to struvite-K ($MgKPO_4{\cdot}6H_2O$, PDF #75-1076, $Pmn2_1$) were identified, corresponding to the *ex situ* XRD data (Figure 2). The calculated unit cell parameters for struvite-K are reported in Table 2, where a = 6.8748(2) Å, b = 6.1658(2) Å, and c = 11.0960(3) Å, which demonstrate good agreement with the reported literature values.[3,5]

At 200 °C, all struvite-K reflections were observed to disappear following the single-step dehydration of struvite-K shown to occur between 50 and 200 °C (Figure 6). At 200 °C, diffuse scattering was observed in the range $25° \leq 2\theta \leq 35°$, which indicated the presence of an amorphous struvite-K dehydration product, of assumed stoichiometry $MgKPO_4$, forming as the initial product of the reaction shown in eq 4. As far as we are aware, this is the first reported evidence for a crystalline to amorphous phase transition in struvite-K, as a consequence of dehydration. We designate this amorphous phase as δ-$MgKPO_4$. Diffuse scattering, and thus the inferred amorphous δ-$MgKPO_4$ phase, was observed between 100 and ≤300 °C, after which crystallization to β-$MgKPO_4$ occurred between 350 and 400 °C. It is therefore likely that the exothermic event observed in Figure 8 was associated with the crystallization of δ-$MgKPO_4$ to β-$MgKPO_4$.

Potassium−magnesium monophosphate, $MgKPO_4$, is reported to occur as three polymorphs: α-$MgKPO_4$ ($P2_1/c$), β-$MgKPO_4$ ($Pna2_1$), and γ-$MgKPO_4$ ($Pnma$),[51−53] with reversible transitions observed on heating leading to stabilized stuffed tridymite structures ($A^+B^{2+}PO_4$).[51] This is supported by DSC data presented in the literature, where two endothermic transitions at 360 and 420 °C were assigned to the first-order transition of α-$MgKPO_4$ to β-$MgKPO_4$ and the second-order transition of β-$MgKPO_4$ to γ-$MgKPO_4$, respectively.[53] In Figure 6A, the latter transition was observed with β-$MgKPO_4$ identified at 350 °C and γ-$MgKPO_4$ above 550 °C. These phase transitions are more readily visible in Figure 6B, where the major reflections ($25° \leq 2\theta \leq 30°$) are presented at 50 °C intervals up to 1000 °C.

The high-temperature $MgKPO_4$ phase assignments of Wallez et al. were based on systematic absences for the orthorhombic $Pna2_1$ (β-$MgKPO_4$) and $Pnma$ (γ-$MgKPO_4$) structures.[51] However, these two space groups cannot be distinguished on the basis of a consideration of systematic absences.[54] To elucidate the structural assignment here, Rietveld refinements were performed on data acquired at 350, 550, and 800 °C. At 350 °C, the β-$MgKPO_4$ ($Pna2_1$) phase was assigned as the most satisfactory fit of reflection intensities (see Rietveld refinement in Figure S2A in the Supporting Information), in comparison to the $Pnma$ γ-$MgKPO_4$ structure (Figure S2B). In contrast, at 550 and 800 °C, the diffraction patterns could only be satisfactorily refined using the $Pnma$ γ-$MgKPO_4$ structure, most notably at 800 °C (Figure S2C).

In this study, the β-$MgKPO_4$ to γ-$MgKPO_4$ transition was observed between 450 and 550 °C, with γ-$MgKPO_4$ present

https://dx.doi.org/10.1021/acs.inorgchem.0c02802
Inorg. Chem. 2021, 60, 195−205

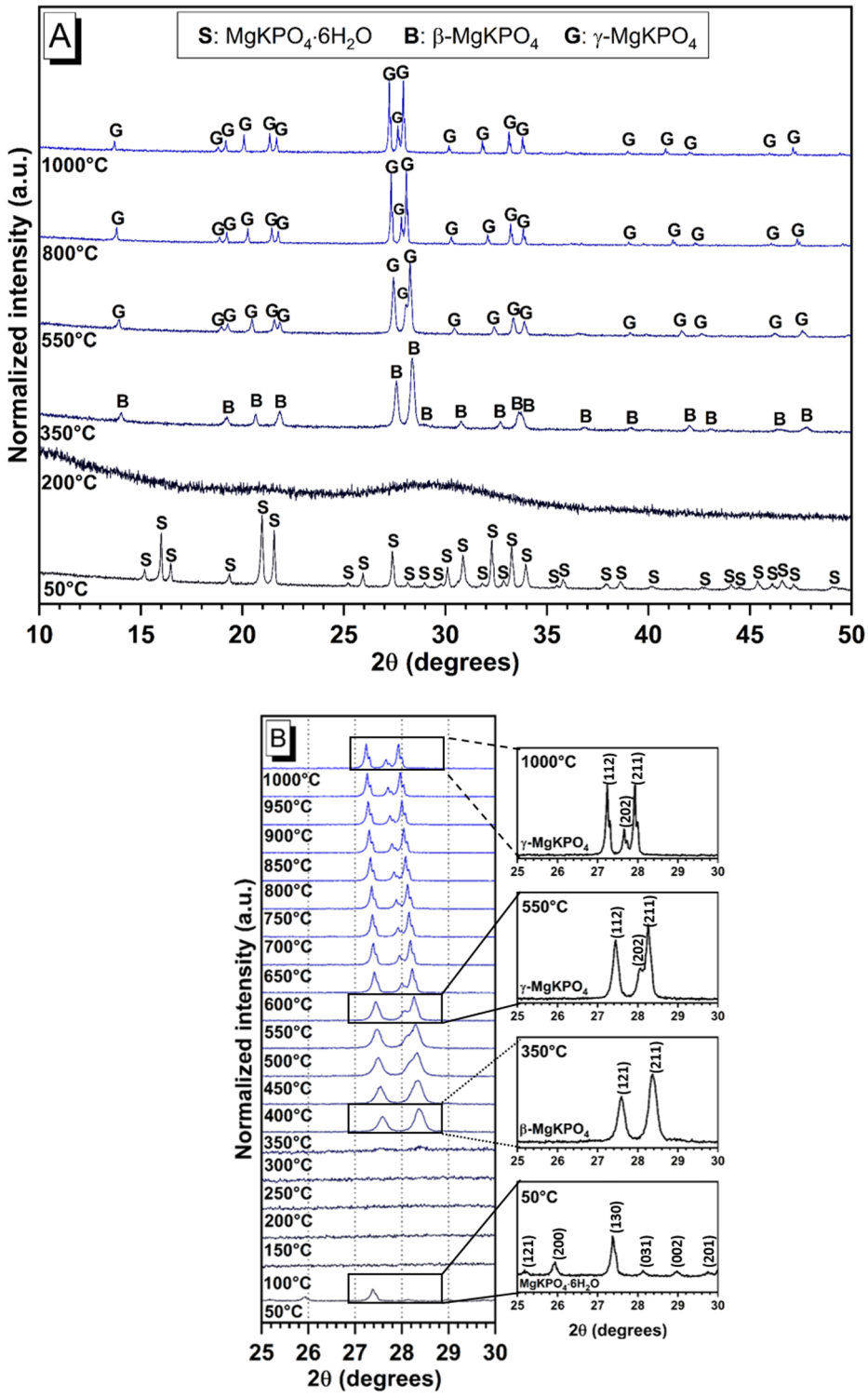

Figure 6. *In situ* HTXRD of struvite-K on heating: (A) up to 1000 °C; (B) at 50 °C increments in the range $25° \leq 2\theta \leq 30°$.

≥550−1000 °C, with thermal expansion resulting in a progressive shift of reflections to lower 2θ values commensurate with observed changes in the unit cell parameters (Table 2) including the unit cell volume, as shown in Figure 7. This was in good agreement with the DSC data of Wallez et al. and Miladi et al., who estimated the β- to γ-$MgKPO_4$ phase transition to occur at ∼420 °C on heating.[51,53] On cooling, a change in the rate of thermal expansion was observed between 350 and 450 °C (Figure 7 and Table 2), consistent with the reverse γ- to β-$MgKPO_4$ transition, which concurs with DSC cooling data, where the transition was observed at ∼415 °C.[53] From single-crystal diffraction data, Wallez et al. proposed that the β- to γ-$MgKPO_4$ transition is second order in nature, involving rotation of the MgO_4 and PO_4 tetrahedra forming six-membered rings, which define one-dimensional tunnels. This results in an increase in ionic conductivity in γ-$MgKPO_4$ arising from hopping of K^+ ions along the one-dimensional tunnels, which are less distorted and are of greater aperture than in β-

https://dx.doi.org/10.1021/acs.inorgchem.0c02802
Inorg. Chem. 2021, 60, 195−205

Table 2. Calculated Unit Cell Parameters for the Key *In Situ* HTXRD Temperatures (Heating and Cooling) as Reported in Figures 6A and 8A

temp (°C)	phase	space group	a (Å)	b (Å)	c (Å)	β (deg)	V (Å^3)	R_{wp} (%)	R_p (%)	χ^2
					Heating					
50	$MgKPO_4{\cdot}6H_2O$	$Pmn2_1$	6.8748(2)	6.1658(2)	11.0960(3)		470.35(2)	7.16	5.36	2.699
350	β-$MgKPO_4$	$Pna2_1$	8.5857(5)	9.2441(6)	5.2948(4)		420.23(3)	6.61	5.14	1.870
550	γ-$MgKPO_4$	$Pnma$	8.6703 (7)	5.2870(4)	9.3532(7)		428.71(8)	5.38	4.19	1.245
800	γ-$MgKPO_4$	$Pnma$	8.7548(1)	5.2928(1)	9.3933(1)		435.26(1)	5.66	4.45	1.347
1000	γ-$MgKPO_4$	$Pnma$	8.8176(2)	5.2914(1)	9.4077(2)		438.94(1)	7.32	5.58	2.133
					Cooling					
800	γ-$MgKPO_4$	$Pnma$	8.7490(2)	5.2888(1)	9.3862(2)		434.32(1)	7.29	5.62	2.054
400	γ-$MgKPO_4$	$Pnma$	8.6031(6)	9.2684(6)	5.2960(3)		422.29(6)	6.73	5.28	1.719
350[a]	β-$MgKPO_4$	$Pna2_1$	8.5843(3)	9.2214(6)	5.3088(3)		420.24(2)	6.80	5.28	1.732
	α-$MgKPO_4$	$P2_1/c$	8.6279(18)	5.1259(10)	18.8923(29)	91.595(12)	835.20(14)			
300	α-$MgKPO_4$	$P2_1/c$	8.6157(3)	5.1241(2)	18.9344(7)	91.651(3)	835.57(0)	6.49	5.10	1.559
50	α-$MgKPO_4$	$P2_1/c$	8.5603(3)	5.0862(2)	18.9887(7)	91.676(3)	826.39(3)	6.48	5.08	1.546

[a]The sample at 350 °C (cooling) contained a mixed-phase assemblage: β-$MgKPO_4$ ($Pna2_1$, 76.11 wt %) and α-$MgKPO_4$ ($P2_1/c$, 23.89 wt %).

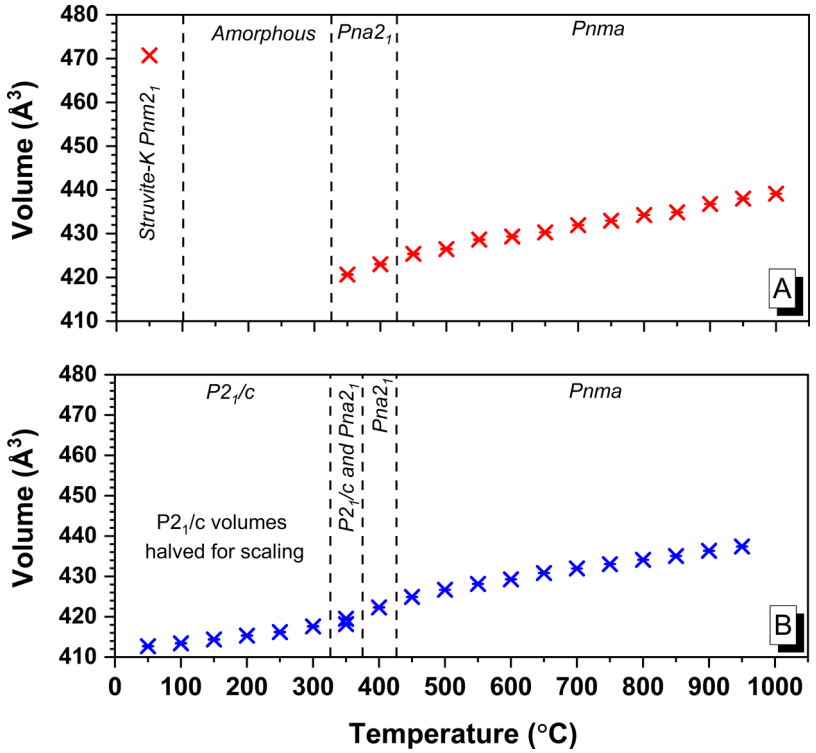

Figure 7. Variation of unit cell volumes with temperature for $MgKPO_4$ (dehydrated struvite-K) on (A) heating and (B) cooling as measured using *in situ* HTXRD. Space groups were identified and labeled with regard to the appropriate temperature range. Refinement errors are presented as error bars calculated during the Le Bail pattern fitting.

$MgKPO_4$,[51] and associated with the subtle change in rate of thermal expansion we observe between 350 and 450 °C.

In situ HTXRD data for struvite-K were also collected on cooling immediately following the heating to 1000 °C (Figure 8); the γ-$MgKPO_4$ phase was observed over the range 1000–450 °C. A comparative Rietveld analysis was undertaken on XRD data acquired at 400 °C, which again favored the $Pna2_1$ β-$MgKPO_4$ structure over $Pnma$ (γ-$MgKPO_4$). This was in agreement with the DSC data of Wallez et al. and Miladi et al., who estimated that the γ- to β-$MgKPO_4$ phase transition on cooling occurred at 419 and 415 °C, respectively.[51,53]

HTXRD data acquired at 350 °C on cooling (Figure 8) could be indexed as comprising both β-$MgKPO_4$ (see inset, $Pna2_1$ (211) and (121) reflections) and α-$MgKPO_4$ (see inset, $P2_1/c$ (114) and (11$\bar{4}$) reflections). HTXRD data acquired at 300 °C and below could be indexed as comprising only the $P2_1/c$ α-$MgKPO_4$ phase. In Figure 7, the unit cell volume for the α-$MgKPO_4$ $P2_1/c$ phase was scaled by half for ease of comparison, accounting for the doubling of the c axis in this phase (also observed in Table 2). It should be noted that α-$MgKPO_4$ was not observed on heating (Figure 6), since the crystallization of amorphous δ-$MgKPO_4$ yields β-$MgKPO_4$. Our observations are broadly consistent with the assignment of the β-$MgKPO_4$ to α-$MgKPO_4$ phase transition at 362 °C on heating and 353 °C on cooling.[51] The observation of an apparent two phase region in our study at 350 °C, on the cusp of the reported phase transition, has not been previously reported. This is considered to be associated with a small temperature gradient across the sample,

https://dx.doi.org/10.1021/acs.inorgchem.0c02802
Inorg. Chem. 2021, 60, 195–205

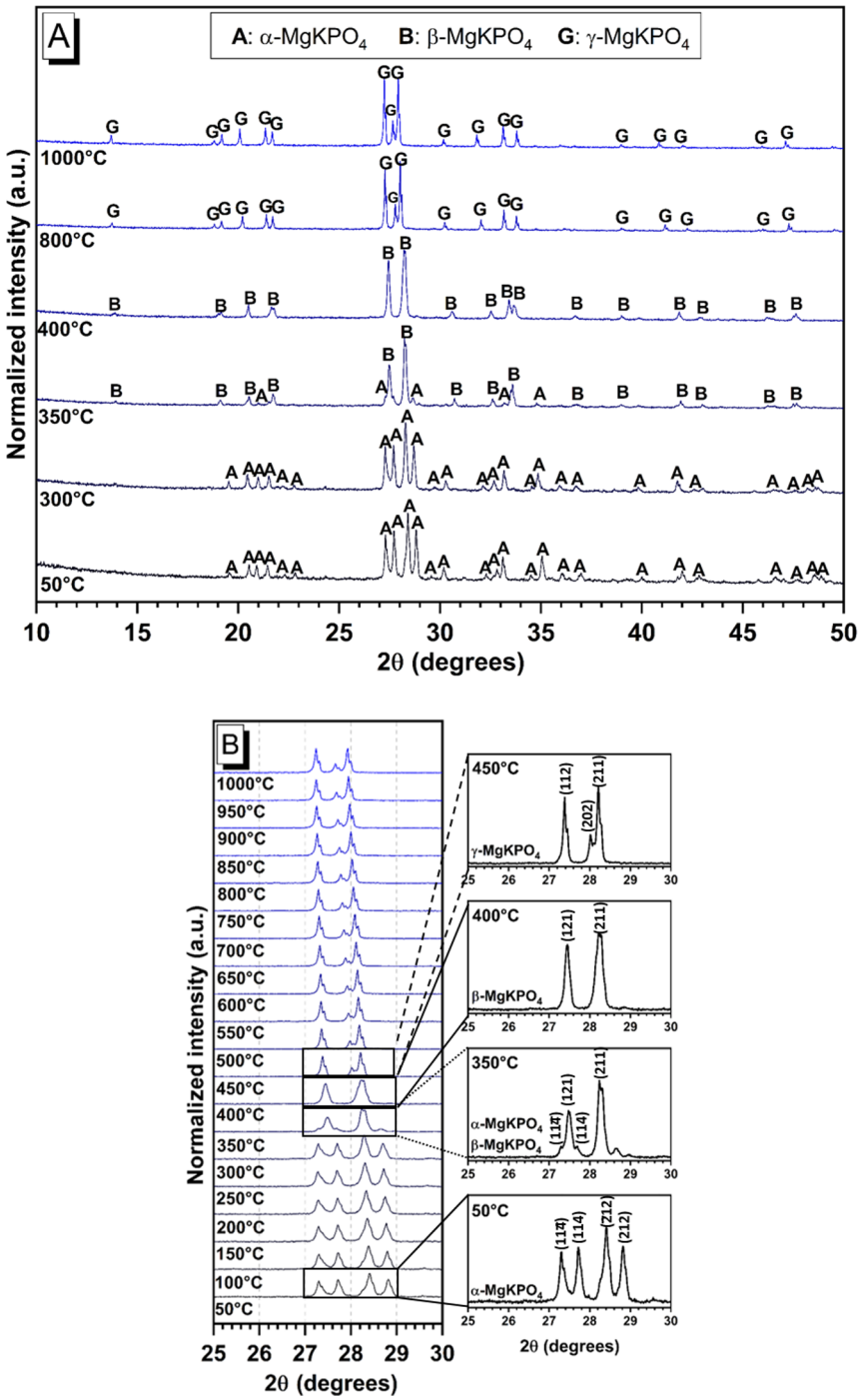

Figure 8. *In situ* HTXRD of struvite-K on cooling: (A) from 1000 to 50 °C; (B) at 50 °C decrements in the range $25° \leq 2\theta \leq 30°$.

where different parts of the sample were at different temperatures, resulting in the detection of both the β- and α-$MgKPO_4$ phases. The phase transition from α-$MgKPO_4$ to β-$MgKPO_4$ is reported to be of first order; in the β phase, Mg is coordinated as MgO_4 polyhedra, whereas on transformation to the α phase, polyhedral tilting results in the formation of MgO_5 polyhedra (arising from sharing of a PO_4 oxygen).[51]

The behavior of struvite-K was dissimilar to the dehydration behavior of struvite, where the simultaneous loss of ammonia and water is observed,[55,56] resulting in the formation of an amorphous $MgHPO_4$ phase between 200 and 700 °C, with crystalline magnesium phosphate phases observed above 700 °C.[56] This could indicate that struvite-K is more resilient to exposure to high temperatures in comparison to the analogous struvite, which could provide potential benefits in comparison to struvite for applications such as fire-resistant coatings and magnesium potassium phosphate cements designed for radioactive waste immobilization.

4. CONCLUSIONS

In this study, high-field solid-state ^{25}Mg and ^{39}K MAS NMR spectra and their corresponding quadrupolar parameters were presented for synthetic struvite-K for the first time. It has been shown experimentally and theoretically that both the Mg and K environments exist as single sites, which is in agreement with the

https://dx.doi.org/10.1021/acs.inorgchem.0c02802
Inorg. Chem. 2021, 60, 195−205

reported crystal structure and existing ^{25}Mg MAS NMR data for isostructural struvite. The behavior of struvite-K was found to undergo a single-step dehydration at <120 °C, leading to the formation of the dehydration product, potassium−magnesium monophosphate ($MgKPO_4$), which was poorly crystalline up to 300 °C, denoted as δ-$MgKPO_4$. Above this temperature, a phase transition to the β-$MgKPO_4$ phase (350 °C) occurred, followed by transition to the γ-$MgKPO_4$ phase upon further heating, confirming literature theory. To the best of our knowledge, this is first report of a crystalline−amorphous−crystalline transition for struvite-K on exposure to high temperature; however, further research would be required to underpin the transition mechanism(s). On cooling, the reverse transition of γ-$MgKPO_4$ to β-$MgKPO_4$ was observed at 400 °C, followed by a second transition between 350 and 300 °C to the α-$MgKPO_4$ phase, which remained dominant at room temperature.

■ ASSOCIATED CONTENT

Supporting Information

The Supporting Information is available free of charge at https://pubs.acs.org/doi/10.1021/acs.inorgchem.0c02802.

SEM/EDX of struvite-K and Rietveld refinement fits at selected temperatures (PDF)

■ AUTHOR INFORMATION

Corresponding Author

Neil C. Hyatt − *Immobilisation Science Laboratory, Department of Materials Science and Engineering, University of Sheffield, Sheffield S1 3JD, U.K.;* orcid.org/0000-0002-2491-3897; Phone: +44 (0) 114 222 5470; Email: n.c.hyatt@sheffield.ac.uk

Authors

Laura J. Gardner − *Immobilisation Science Laboratory, Department of Materials Science and Engineering, University of Sheffield, Sheffield S1 3JD, U.K.;* orcid.org/0000-0003-3126-2583

Samuel A. Walling − *Immobilisation Science Laboratory, Department of Materials Science and Engineering, University of Sheffield, Sheffield S1 3JD, U.K.*

Sebastian M. Lawson − *Immobilisation Science Laboratory, Department of Materials Science and Engineering, University of Sheffield, Sheffield S1 3JD, U.K.;* orcid.org/0000-0003-4786-6947

Shikuan Sun − *Immobilisation Science Laboratory, Department of Materials Science and Engineering, University of Sheffield, Sheffield S1 3JD, U.K.;* orcid.org/0000-0002-1688-5072

Susan A. Bernal − *Immobilisation Science Laboratory, Department of Materials Science and Engineering, University of Sheffield, Sheffield S1 3JD, U.K.*

Claire L. Corkhill − *Immobilisation Science Laboratory, Department of Materials Science and Engineering, University of Sheffield, Sheffield S1 3JD, U.K.;* orcid.org/0000-0002-7488-3219

John L. Provis − *Immobilisation Science Laboratory, Department of Materials Science and Engineering, University of Sheffield, Sheffield S1 3JD, U.K.;* orcid.org/0000-0003-3372-8922

David C. Apperley − *Department of Chemistry, Durham University, Durham DH1 3LE, U.K.*

Dinu Iuga − *Department of Physics, University of Warwick, Coventry CV4 7AL, U.K.*

John V. Hanna − *Department of Physics, University of Warwick, Coventry CV4 7AL, U.K.;* orcid.org/0000-0002-0644-3932

Complete contact information is available at: https://pubs.acs.org/10.1021/acs.inorgchem.0c02802

Notes

The authors declare no competing financial interest.

■ ACKNOWLEDGMENTS

L.J.G. is grateful to the Nuclear Decommissioning Authority (NDA) for a Ph.D. sponsorship, under supervision by the National Nuclear Laboratory. N.C.H. wishes to acknowledge the Royal Academy of Engineering and the NDA for funding and the EPSRC for partial support under grant references EP/S032959/1, EP/P013600/1, and EP/N017617/1. N.C.H., S.A.W., and S.M.L. are grateful to the EPSRC for provision of a CDT Ph.D. studentship under grant reference EP/G037140/1. C.L.C. is grateful to the University of Sheffield for the award of a Vice Chancellor's fellowship and the EPSRC for the award of an Early Career Fellowship under grant reference EP/N017374/1. The authors thank Dr. Nik Reeves-McLaren for support collecting *in situ* high-temperature XRD data. Solid-state NMR spectra (^{31}P) were obtained at the EPSRC UK National Solid-State NMR Service at Durham. The UK 850 MHz Solid-State NMR Facility used in this research (^{25}Mg, ^{39}K) was funded by the EPSRC and BBSRC, as well as the University of Warwick, including via partial funding through Birmingham Science City Advanced Materials Projects 1 and 2 supported by Advantage West Midlands (AWM) and the European Regional Development Fund (ERDF). This research utilized the HADES/MIDAS facility at the University of Sheffield established with financial support from the EPSRC and BEIS, under grant EP/T011424/1.[57]

■ REFERENCES

(1) Ulex, G. L. Clxiii. On Struvite, A New Mineral. *Memoirs and Proceedings of the Chemical Society* **1845**, *3* (0), 106−110.

(2) Whitaker, A.; Jeffery, J. W. The Crystal Structure of Struvite, $MgNH_4PO_4{\cdot}6H_2O$. *Acta Crystallogr., Sect. B: Struct. Crystallogr. Cryst. Chem.* **1970**, *26* (10), 1429−1440.

(3) Mathew, M.; Schroeder, L. W. Crystal Structure of a Struvite Analogue, $MgKPO_4{\cdot}6H_2{\cdot}O$. *Acta Crystallogr., Sect. B: Struct. Crystallogr. Cryst. Chem.* **1979**, *35* (1), 11−13.

(4) Banks, E.; Chianelli, R.; Korenstein, R. Crystal Chemistry of Struvite Analogs of the Type $MgMPO_4{\cdot}6H_2O$ ($M^+ = K^+$, Rb^+, Cs^+, Tl^+, NH_4^+). *Inorg. Chem.* **1975**, *14* (7), 1634−1639.

(5) Graeser, S.; Postl, W.; Bojar, H.-P.; Berlepsch, P.; Armbruster, T.; Raber, T.; Ettinger, K.; Walter, F. Struvite-(K), $KMgPO_4{\cdot}6H_2O$, The Potassium Equivalent of Struvite − A New Mineral. *Eur. J. Mineral.* **2008**, *20* (4), 629−633.

(6) Momma, K.; Izumi, F. VESTA 3 for Three-Dimensional Visualization of Crystal, Volumetric and Morphology Data. *J. Appl. Crystallogr.* **2011**, *44* (6), 1272−1276.

(7) Walling, S. A.; Provis, J. L. Magnesia Based Cements − A Journey of 150 Years, and Cements For The Future? *Chem. Rev.* **2016**, *116* (7), 4170−4204.

(8) Singh, D.; Wagh, A. S.; Tlustochowicz, M.; Jeong, S. Y. Phosphate Ceramic Process for Macroencapsulation And Stabilization of Low-Level Debris Wastes. *Waste Manage.* **1998**, *18* (2), 135−143.

(9) Cau Dit Coumes, C.; Lambertin, D.; Lahalle, H.; Antonucci, P.; Cannes, C.; Delpech, S. Selection of a Mineral Binder with Potentialities for the Stabilization/Solidification of Aluminum Metal. *J. Nucl. Mater.* **2014**, *453* (1), 31−40.

(10) Lahalle, H.; Cau Dit Coumes, C.; Mesbah, A.; Lambertin, D.; Cannes, C.; Delpech, S.; Gauffinet, S. Investigation of magnesium phosphate cement hydration in diluted suspension and its retardation by boric acid. *Cem. Concr. Res.* **2016**, *87*, 77−86.
(11) Covill, A. *Novel encapsulants for intermediate level waste in the UK nuclear industry*; Department of Materials Science and Engineering, University of Sheffield: 2010.
(12) Hayes, M.; Godfrey, I. H. In *Development of the use of alternative cements for the treatment of intermediate level waste*; Waste Management Symposia Proccedings, Feb 25−Mar 1, 2007; pp 1−14.
(13) Singh, D.; Mandalika, V. R.; Parulekar, S. J.; Wagh, A. S. Magnesium potassium phosphate ceramic for ^{99}Tc immobilization. *J. Nucl. Mater.* **2006**, *348* (3), 272−282.
(14) Gardner, L. J.; Bernal, S. A.; Walling, S. A.; Corkhill, C. L.; Provis, J. L.; Hyatt, N. C. Characterisation of magnesium potassium phosphate cements blended with fly ash and blast furnace slag. *Cem. Concr. Res.* **2015**, *74*, 78−87.
(15) Ahmad, M. R.; Chen, B.; Yu, J. A comprehensive study of basalt fiber reinforced magnesium phosphate cement incorporating ultrafine fly ash. *Composites, Part B* **2019**, *168*, 204−217.
(16) Fang, Y.; Cui, P.; Ding, Z.; Zhu, J.-X. Properties of a magnesium phosphate cement-based fire-retardant coating containing glass fiber or glass fiber powder. *Construction and Building Materials* **2018**, *162*, 553−560.
(17) Feng, H.; Sheikh, M. N.; Hadi, M. N. S.; Gao, D.; Zhao, J. Mechanical properties of micro-steel fibre reinforced magnesium potassium phosphate cement composite. *Construction and Building Materials* **2018**, *185*, 423−435.
(18) Amiandamhen, S. O.; Montecuccoli, Z.; Meincken, M.; Barbu, M. C.; Tyhoda, L. Phosphate bonded wood composite products from invasive Acacia trees occurring on the Cape Coastal plains of South Africa. *European Journal of Wood and Wood Products* **2018**, *76* (2), 437−444.
(19) Kim, H.; Han, D.; Kim, K.; Romero, P. Performance assessment of repair material for deteriorated concrete slabs using chemically bonded cement. *Construction and Building Materials* **2020**, *237*, 117468.
(20) Jia, X.; Li, J.; Wang, P.; Qian, J.; Tang, M. Preparation and mechanical properties of magnesium phosphate cement for rapid construction repair in ice and snow. *Construction and Building Materials* **2019**, *229*, 116927.
(21) Park, J. W.; Kim, K. H.; Ann, K. Y. Fundamental Properties of Magnesium Phosphate Cement Mortar for Rapid Repair of Concrete. *Advances in Materials Science and Engineering* **2016**, *2016*, 7.
(22) Du, Y.-J.; Wei, M.-L.; Reddy, K. R.; Wu, H.-l. Effect of carbonation on leachability, strength and microstructural characteristics of KMP binder stabilized Zn and Pb contaminated soils. *Chemosphere* **2016**, *144*, 1033−1042.
(23) Feng, Y.-S.; Du, Y.-J.; Reddy, K. R.; Xia, W.-Y. Performance of two novel binders to stabilize field soil with zinc and chloride: Mechanical properties, leachability and mechanisms assessment. *Construction and Building Materials* **2018**, *189*, 1191−1199.
(24) Huang, H.; Li, J.; Li, B.; Zhang, D.; Zhao, N.; Tang, S. Comparison of Different K-Struvite Crystallization Processes for Simultaneous Potassium and Phosphate Recovery from Source-Separated Urine. *Sci. Total Environ.* **2019**, *651*, 787−795.
(25) Xu, K.; Zhang, C.; Li, J.; Cheng, X.; Wang, C. Removal and Recovery Of N, P and K from Urine *via* Ammonia Stripping and Precipitations of Struvite and Struvite-K. *Water Sci. Technol.* **2017**, *75* (1), 155−164.
(26) Randall, D. G.; Naidoo, V. Urine: The Liquid Gold of Wastewater. *J. Environ. Chem. Eng.* **2018**, *6* (2), 2627−2635.
(27) Iuga, D.; Kentgens, A. P. M. Influencing the satellite transitions of half-integer quadrupolar nuclei for the enhancement of magic angle spinning spectra. *J. Magn. Reson.* **2002**, *158* (1), 65−72.
(28) Laurencin, D.; Gervais, C.; Stork, H.; Krämer, S.; Massiot, D.; Fayon, F. ^{25}Mg Solid-State NMR of Magnesium Phosphates: High Magnetic Field Experiments and Density Functional Theory Calculations. *J. Phys. Chem. C* **2012**, *116* (37), 19984−19995.
(29) Hahn, E. L. Spin Echoes. *Phys. Rev.* **1950**, *80* (4), 580−594.
(30) Duxson, P.; Provis, J. L.; Lukey, G. C.; van Deventer, J. S. J.; Separovic, F.; Gan, Z. H. ^{39}K NMR of Free Potassium in Geopolymers. *Ind. Eng. Chem. Res.* **2006**, *45* (26), 9208−9210.
(31) *TopSpin 3.2*; Bruker: 2013.
(32) Ait Benhamou, R.; Wallez, G.; Loiseau, P.; Viana, B.; Elaatmani, M.; Daoud, M.; Zegzouti, A. Polymorphism of New Rubidium Magnesium Monophosphate. *J. Solid State Chem.* **2010**, *183* (9), 2082−2086.
(33) Yamashita, I.; Kawaji, H.; Atake, T.; Kuroiwa, Y.; Sawada, A. Order-Disorder Mechanism of the I-II Phase Transition in $CsZnPO_4$. *Phys. Rev. B: Condens. Matter Mater. Phys.* **2003**, *67* (1), 014104.
(34) Scrimgeour, S. N.; Chudek, J. A.; Cowper, G. A.; Lloyd, C. H. ^{31}P Solid-State MAS-NMR Spectroscopy of the Compounds that form in Phosphate-Bonded Dental Casting Investment Materials During Setting. *Dent. Mater.* **2007**, *23* (8), 934−943.
(35) Ma, N.; Rouff, A. A.; Phillips, B. L. A ^{31}P NMR and TG/DSC-FTIR Investigation of the Influence of Initial pH on Phosphorus Recovery as Struvite. *ACS Sustainable Chem. Eng.* **2014**, *2* (4), 816−822.
(36) Connaway-Wagner, M. C.; Klemperer, W. G.; Young, J. F. In *Advances in Cementitious Materials*; Mindess, S., Ed.; The American Ceramic Society: Westerville, OH, 1991; Chapter 679−688, Vol. *16*.
(37) Ashbrook, S. E.; Sneddon, S. New Methods and Applications in Solid-State NMR Spectroscopy of Quadrupolar Nuclei. *J. Am. Chem. Soc.* **2014**, *136* (44), 15440−15456.
(38) Khan, A. A.; Baur, W. H. Salt Hydrates. VII. The Crystal Structures of Sodium Ammonium Orthochromate Dihydrate and Magnesium Diammonium Bis(Hydrogen Orthophosphate) Tetrahydrate and A Discussion Of The Ammonium Ion. *Acta Crystallogr., Sect. B: Struct. Crystallogr. Cryst. Chem.* **1972**, *28* (3), 683−693.
(39) Shannon, R. Revised Effective Ionic Radii and Systematic Studies of Interatomic Distances in Halides and Chalcogenides. *Acta Crystallogr., Sect. A: Cryst. Phys., Diffr., Theor. Gen. Crystallogr.* **1976**, *32* (5), 751−767.
(40) Zhang, S.; Shi, H.; Huang, S.; Zhang, P. Dehydration Characteristics of Struvite-K Pertaining to Magnesium Potassium Phosphate Cement System in Non-Isothermal Condition. *J. Therm. Anal. Calorim.* **2013**, *111*, 35−40.
(41) Chauhan, C. K.; Vyas, P. M.; Joshi, M. J. Growth and Characterization of Struvite-K Crystals. *Cryst. Res. Technol.* **2011**, *46* (2), 187−194.
(42) Ma, H.; Xu, B.; Li, Z. Magnesium Potassium Phosphate Cement Paste: Degree of Reaction, Porosity and Pore Structure. *Cem. Concr. Res.* **2014**, *65* (0), 96−104.
(43) Chong, L.; Yang, J.; Shi, C. Effect of Curing Regime on Water Resistance of Magnesium−Potassium Phosphate Cement. *Construction and Building Materials* **2017**, *151*, 43−51.
(44) Xu, B.; Lothenbach, B.; Ma, H. Properties of Fly Ash Blended Magnesium Potassium Phosphate Mortars: Effect of the Ratio Between Fly Ash and Magnesia. *Cem. Concr. Compos.* **2018**, *90*, 169−177.
(45) Gardner, L. J.; Corkhill, C. L.; Walling, S. A.; Bernal, S. A.; Vigor, J. E.; Murray, C. A.; Tang, C. C.; Provis, J. L.; Hyatt, N. C. Early Age Hydration and Aplication of Blended Magneisum Potassium Phosphate Cements for Reduced Corrosion of Reactive Metals. *Cem. Concr. Res.* **2020**, under review.
(46) Ding, Z.; Li, Z. Effect of Aggregates and Water Contents on the Properties of Magnesium Phospho-Silicate Cement. *Cem. Concr. Compos.* **2005**, *27* (1), 11−18.
(47) Wagh, A. S.; Strain, R.; Jeong, S. Y.; Reed, D.; Krause, T.; Singh, D. Stabilization of Rocky Flats Pu-Contaminated Ash within Chemically Bonded Phosphate Ceramics. *J. Nucl. Mater.* **1999**, *265* (3), 295−307.
(48) Covill, A.; Hyatt, N. C.; Hill, J.; Collier, N. C. Development of Magnesium Phosphate Cements for Encapsulation of Radioactive Waste. *Adv. Appl. Ceram.* **2011**, *110* (3), 151−156.
(49) Le Rouzic, M.; Chaussadent, T.; Platret, G.; Stefan, L. Mechanisms of K-Struvite Formation in Magnesium Phosphate Cements. *Cem. Concr. Res.* **2017**, *91*, 117−122.

https://dx.doi.org/10.1021/acs.inorgchem.0c02802
Inorg. Chem. 2021, 60, 195−205

(50) Mo, L.; Lv, L.; Deng, M.; Qian, J. Influence of Fly Ash and Metakaolin on the Microstructure and Compressive Strength of Magnesium Potassium Phosphate Cement PWaste. *Cem. Concr. Res.* **2018**, *111*, 116−129.
(51) Wallez, G.; Colbeau-Justin, C.; Le Mercier, T.; Quarton, M.; Robert, F. Crystal Chemistry and Polymorphism of Potassium−Magnesium Monophosphate. *J. Solid State Chem.* **1998**, *136* (2), 175−180.
(52) Miladi, L.; Oueslati, A.; Guidara, K. Vibrational Spectroscopic and Dielectric Properties Investigations of Phase Transitions in $KMgPO_4$ Compound. *J. Mol. Struct.* **2017**, *1148*, 404−411.
(53) Miladi, L.; Oueslati, A.; Guidara, K. Phase Transition, Conduction Mechanism and Modulus Study of $KMgPO_4$ Compound. *RSC Adv.* **2016**, *6* (86), 83280−83287.
(54) Marsh, R. Some Thoughts on Choosing the Correct Space Group. *Acta Crystallogr., Sect. B: Struct. Sci.* **1995**, *51* (6), 897−907.
(55) Sarkar, A. K. Hydration/Dehydration Characteristics of Struvite and Dittmarite Pertaining to Magnesium Ammonium Phosphate Cement Systems. *J. Mater. Sci.* **1991**, *26* (9), 2514−2518.
(56) Bhuiyan, M. I. H.; Mavinic, D. S.; Koch, F. A. Thermal Decomposition of Struvite and its Phase Transition. *Chemosphere* **2008**, *70* (8), 1347−1356.
(57) Hyatt, N. C.; Corkhill, C. L.; Stennett, M. C.; Hand, R. J.; Gardner, L. J.; Thorpe, C. L. The HADES facility for high activity decommissioning engineering & science: Part of the UK national nuclear user facility. *IOP Conf. Ser.: Mater. Sci. Eng.* **2020**, *818*, 012022.

https://dx.doi.org/10.1021/acs.inorgchem.0c02802
Inorg. Chem. 2021, 60, 195−205